

Evaluation of Protein Adsorption on Atmospheric Plasma Deposited Coatings Exhibiting Superhydrophilic to Superhydrophobic Properties

C. P. Stallard · K. A. McDonnell · O. D. Onayemi ·
J. P. O'Gara · D. P. Dowling

Received: 2 March 2012 / Accepted: 5 April 2012 / Published online: 3 May 2012
© The Author(s) 2012. This article is published with open access at Springerlink.com

Abstract Protein adsorption is one of the key parameters influencing the biocompatibility of medical device materials. This study investigates serum protein adsorption and bacterial attachment on polymer coatings deposited using an atmospheric pressure plasma jet system. The adsorption of bovine serum albumin and bovine fibrinogen (Fg) onto siloxane and fluorinated siloxane elastomeric coatings that exhibit water contact angles (θ) ranging from superhydrophilic ($\theta < 5^\circ$) to superhydrophobic ($\theta > 150^\circ$) were investigated. Protein interactions were evaluated in situ under dynamic flow conditions by spectroscopic ellipsometry. Superhydrophilic coatings showed lower levels of protein adsorption when compared with hydrophobic siloxane coatings, where preferential adsorption was shown to occur. Reduced levels of protein adsorption were also observed on fluorinated siloxane copolymer coatings exhibiting hydrophobic wetting behaviour. The lower levels of protein adsorption observed on these surfaces indicated that the presence of fluorocarbon groups have the effect of reducing surface affinity for protein attachment. Analysis of superhydrophobic siloxane and fluorosiloxane surfaces showed minimal indication of protein adsorption. This was confirmed by bacterial attachment studies using a *Staphylococcus aureus* strain known to bind specifically to Fg, which showed almost no attachment to the superhydrophobic coating after protein adsorption experiments. These results showed the superhydrophobic surfaces to

exhibit antimicrobial properties and significantly reduce protein adsorption.

1 Introduction

When a biomaterial is introduced into the body interactions take place between the first few nanometres of the material surface and the surrounding tissue or body fluid [1]. The adsorption of a protein layer is the first stage in this response which can then function to mediate cellular adhesion and as a result is an important issue when considering the design of implant materials. The formation of a protein layer can induce implant failure by both promoting bacterial adhesion and facilitating the formation of thrombin [2, 3]. In these instances protein attachment initiates failure cascades which can lead to inflammation and immune reaction, causing a loss of biocompatibility and functionality [4]. A number of approaches have been applied to tailor polymer and metal surfaces for biomedical applications and to study the adhesion of proteins. Some of these include the use of graft polymerisation [5], and plasma modification techniques such as ion beam implantation and plasma polymerisation [6, 7]. The atmospheric pressure plasma technique examined in this study can be employed as a post production process for surface modification of sensitive materials under low temperature ambient conditions.

Protein adsorption is influenced by the particular physico-chemical properties of the biomaterial surface which include chemistry, wettability; charge, and surface morphology [8]. The wettability of a material surface is considered to be one of the most influential parameters affecting protein adsorption with numerous studies in particular investigating protein adsorption and cellular

C. P. Stallard · K. A. McDonnell · D. P. Dowling (✉)
UCD School of Mechanical and Materials Engineering,
University College Dublin, Belfield, Dublin 4, Ireland
e-mail: denis.dowling@ucd.ie

O. D. Onayemi · J. P. O'Gara
UCD School of Biomolecular and Biomedical Science,
University College Dublin, Belfield, Dublin 4, Ireland

adhesion on surfaces with a designed wettability gradient [9–12]. It is generally considered that proteins tend to adsorb more favourably onto hydrophobic than hydrophilic surfaces. Both Lee [13] and Xu [12] treated polyethylene material with a glow discharge plasma to produce surfaces with a wettability gradient for the study of albumin and fibrinogen (Fg) adsorption. These studies showed an increased amount of protein adsorption on hydrophobic surfaces and in the latter case, higher protein adhesion forces as surface hydrophobicity increased. Malmsted [14] and Nygren [15] used spectroscopic ellipsometry to monitor the adsorption of serum proteins onto hydrophilic and hydrophobic modified silica surfaces. The study by Malmsted showed higher levels of protein adsorption on hydrophobic substrates which included albumin and fibrinogen, while Nygren et al. also showed higher levels of protein binding on hydrophobic surfaces.

While most literature suggests that protein adsorption tends to occur more favourably on hydrophobic surfaces or on surfaces with an intermediate wettability (60–90°), other investigations have demonstrated more favourable protein adsorption on hydrophilic surfaces [16]. This conflicting data with regard to the influence of surface wetting on protein adsorption is considered to be the result of the variety of factors which influence protein adsorption, including surface charge, roughness, environmental pH, etc. An investigation of albumin and fibronectin (Fn) adsorption by Tamada et al. [17] on polymeric substrates with water contact angles between 20° and 120° observed the highest level of adsorption in the region of 60–80°. A significant drop in protein adsorption was observed as contact angles reduced from 60 to 20°, while surfaces with water contact angles approaching 120° also exhibited a reduction in protein adsorption. There has, however, been relatively few reports on protein adsorption measurements on highly hydrophobic or superhydrophobic ($\theta > 150^\circ$) surfaces. Some researchers report on the adsorption of protein on superhydrophobic surfaces [18] while some report on non-adsorbent properties on these surfaces [19, 20]. Roach et al. studied the interaction of proteins on hydrophilic and superhydrophobic porous thermally modified silica [20]. In their study a reduction in the level of BSA adsorption was observed on the superhydrophobic silica substrate material when compared with hydrophilic substrates. Both hydrophobic and hydrophilic surfaces offer diverse polar interactions for the investigation of protein adsorption. However, the interfacial boundary structure formed when a superhydrophobic surface is contacted with water offers a very different arrangement through which protein molecules must diffuse in order to adsorb to the underlying material surface.

The adsorption of proteins at a biomaterial interface is a dynamic process with attachment, detachment and

conformational changes all often taking place in a flowing aqueous environment. Under laboratory test conditions it is beneficial to replicate this in vivo flow environment where possible. There are many methods of measuring this adsorption, such as surface plasmon resonance (SPR), quartz crystal microbalance (QCM) and radiolabelling techniques. Spectroscopic ellipsometry allows real time in situ monitoring of the process of protein adsorption under flow conditions and has been used to study the thickness, adsorption and desorption kinetics of serum proteins on a range of surface chemistries [14, 21, 22].

The objective of this study is to quantify the adsorption of serum proteins and bacterial attachment on nanometre thick polymer coatings exhibiting water contact angles between $<5^\circ$ and 155° . Analysis of both BSA and Fg was carried out as they are two of the most abundant proteins in blood plasma and have significantly different molecular weights and shapes. Albumin with a molecular weight of 66 kDa is the most abundant plasma protein (50–60 %) and is associated with the transportation of other proteins [23]. It has a heart shaped structure consisting primarily of α -helices 67 %. Fg with a molecular weight of 340 kDa, is a much larger protein, 47 nm in length and consists of three globular domains connected by thin identical sequences [24]. Fg is investigated as it is the protein most associated with the coagulation cascade [29] and is reported to be the dominant ligand promoting attachment of *Staphylococcus aureus* (*S. aureus*), the primary bacteria associated with biomaterial implant related infection [25].

2 Experimental

2.1 Materials

Plasma polymerised siloxane coatings were deposited on one-side polished, p-type, boron doped silicon wafers, resistivity 0–100 Ω cm (450 μ m thick), supplied by Compart Technology Ltd and onto titanium grade 5 coupons (Ti6Al4V—medical grade). The wafers and coupons were ultrasonically cleaned in methanol followed by acetone and propanol, air dried and pretreated with He/O₂ plasma prior to coating deposition using the PlasmaStream™ system [26].

Siloxane monomers were investigated as these chemistries are widely used in plasma polymerisation deposition studies and are considered to be biochemically inert, while offering structural stability and flexibility. Siloxane coatings were deposited from tetramethylethosilicate (TEOS) (C₈H₂₀O₄Si) (Fluka 99 %) and from hexamethyldisiloxane (HMDSO) O(Si(CH₃)₃)₂ (Aldrich 98 %), while fluorinated siloxane coatings (TCFS) were deposited from an equal volume mixture of tetramethylcyclotetrasiloxane

(TMCTS) ((HSiCH₃O)₄) (Aldrich 99 %) and perfluorooctyltriethoxysilane (PFOTES) (C₁₄H₁₉F₁₃O₃Si) (Aldrich 98 %).

Bovine fibrinogen (Fg, type I S, lyophilized powder) and bovine serum albumin (BSA, fraction V, lyophilized powder) were obtained from Sigma and used as received. Phosphate buffered saline (PBS) was freshly prepared using sodium salts: NaH₂PO₄ and Na₂HPO₄ (200 mmol phosphate) and NaCl (100 mmol) obtained from Aldrich to give pH 7.4 at 25 °C. BSA protein solution was prepared at a concentration of 10 mg ml⁻¹ prior to adsorption experiments. Fg protein solutions were prepared at a concentration of 0.1 mg ml⁻¹ by heating the PBS solution to 37 °C and gently stirring after addition of Fg until a slightly hazy solution was obtained.

2.2 Plasma Polymerisation of Functional Coatings

The coatings were deposited using a non-thermal atmospheric plasma jet system which has been described in detail elsewhere [26]. Briefly, the system is configured with a dielectric head housing two pin electrodes either side of a pneumatic nebuliser (Burgener Ari Mist nebuliser) through which liquid chemical precursors are introduced at 80 psi. The chemical precursor interacts with plasma species generated by gas carriers from either a He/O₂ or He/N₂ gas mixture inside a 75 mm long by 15 mm wide Teflon tube. This interaction which initiates polymerisation reactions results in the deposition of cross-linked polymerised coatings downstream of the plasma jet onto substrates positioned beneath the plasma plume. Low frequency electrical power is delivered to both electrodes from a modified PTI 100 W rf power supply at a frequency of approximately 15–25 kHz. Voltage measurements obtained using a custom-built HV probe. The depositions reported in this study were carried out at approximately 13.5 kV. The entire plasma device was moved over the surface of the substrate in a raster pattern (XY directional scan) using a CNC device with a line speed of 15 mm/s and a step interval of 2.5 mm.

2.3 Coating Characterisation

Static water contact angle and surface energy measurements were carried out using the sessile drop technique at room temperature (OCA 20 from Dataphysics Instruments). Deionised water, diiodomethane and ethylene glycol were used for surface energy measurements. Contact angles were determined at three different locations per sample. These were averaged and the OWRK (Owens, Wendt, Rabel and Kaelbe) method was then used to calculate the surface energy of the deposited coatings [21, 22]. The water contact angle and surface energy of the

deposited coatings were determined on five different sample substrates for each coating process condition. The quoted contact angle values (Table 2) represent the mean of these five measurements, and a typical deviation from the mean value of 3° was determined.

The coating surface morphology was examined using a Wyko NT1100 optical profilometer operating in vertical scanning interferometry (VSI) mode. This system was used to calculate the average surface roughness, R_a (arithmetic average roughness) and R_q (root mean square roughness). The thickness of superhydrophobic coatings was determined by step height measurements using this technique. These measurements were facilitated by masking part of the wafer surface with scotch tape prior to coating deposition; this was then removed after coating deposition to obtain a defined coating edge profile. The quoted roughness values (Table 3) represent the average of five measurements, with a typical deviation of 1 and 5 nm for siloxane and fluorinated siloxane, respectively, determined.

Average coating thickness of non-superhydrophobic samples was also measured using an M-2000[®] variable angle spectroscopic ellipsometer from J. A. Woollam Co., utilising an FLS 300 75W Xenon arc lamp operating within a wavelength range of 270–1,700 nm. Three measurements were taken on each sample at incident angles of 65°, 70° and 75°. Analysis of spectroscopic data was carried out using CompleteEase[™] analysis software. It was not possible to use the ellipsometry technique to obtain thickness measurements of the superhydrophobic coatings as the signal from the relatively rough surface morphology was depolarised and did not allow for an accurate model fit for coating thickness.

Fourier transform infrared spectroscopy (FTIR) measurements were carried out on each of the coatings using a Bruker Vertex-70 system. The sample chamber was purged by N₂ gas before the scans were obtained. Spectra were collected in the range of 400–4,000 cm⁻¹ using a spectral resolution of 4 cm⁻¹. The transmission spectra of the coated silicon substrates were obtained by the overlay of 64 scans to increase the signal to noise ratio.

2.4 Protein Adsorption by Spectroscopic Ellipsometry

Protein adsorption analysis was performed by spectroscopic ellipsometry using a specifically designed 5 ml LiquidCell[™] (TLC-100-02.04) supplied by J. A. Woollam. The samples were sealed inside the liquid cell and positioned on the ellipsometry stage. Variation in polarised light was monitored at a fixed incident angle of 70°.

Adsorption tests were carried out on both coated and uncoated silicon wafer substrates (25 mm × 60 mm). The PBS solution was passed through an inlet filter (Acrosdisc Supor, Pore size 5 μm) into the cell using a piezoelectric

micropump, (ThinXSS) operating at a flow rate of 2 ml min^{-1} . To establish a baseline signal PBS was allowed to flow for 10 min prior to introduction of the protein solution. Spectroscopic data relating to both the change in phase, (Δ) and change in amplitude (Ψ), of the light reflected from the housed sample was measured until a signal saturation plateau was observed. After surface saturation, the cell was flushed for 10 min with PBS to remove any loosely bound protein and for a further 10 min with deionised water. On completion of each liquid cell experiment, the cell and lines were flushed with SDS solution followed by deionised water. Signal data was analysed over a reduced spectral wavelength range of 300–900 nm due to protein absorption in the UV region and water absorption in the IR region. Prior to the protein adsorption experiments the thickness and complex refractive index of the coated and uncoated surfaces was determined in both air and PBS ambient media by fitting the data to a Cauchy dispersion function [23].

$$n = A_n + \frac{B_n}{\lambda^2} + \frac{C_n}{\lambda^4},$$

Through regression analysis the optical model is adjusted to find the optical constants and layer thickness that generate data curves that best match the experimental data distribution as indicated by low mean square error statistics. This function was applied to relate the change in the optical parameters measured at the coated substrate surface to the thickness change due to the adsorbing protein layer (d_{el}). The experimental data was fit to a five layer optical model consisting of bulk silicon, silicon oxide, deposited coating, protein layer and ambient medium. Protein film thickness (d_{el}) was modelled using $A_n = 1.45$, $B_n = 0.001$, $C_n = 0$, along with an extinction coefficient (k) of zero. The value of the refractive index of the protein film (n_p) at 633 nm was determined to be 1.465, which is typical of adsorbing thin protein films [15]. The adsorbed protein mass per unit area, or surface concentration Γ , was then calculated according to de Feijter et al. [27].

$$\Gamma = d_{el} \left\{ \frac{(n_f - n_m)}{dn/dc} \right\}$$

where n_f denotes the refractive index of the protein film, n_m , the refractive index of the aqueous medium and dn/dc denotes the refractive index increment of a protein solution with concentration. Values of 1.335 and 1.465 were taken for the refractive index of the buffer and protein film respectively and dn/dc was taken as $0.187 \text{ cm}^3 \text{ g}^{-1}$, which is a typical value for various serum proteins [28]. As ellipsometry analysis is performed on a limited spot size and the modelled layer assumes a homogenous film, a minimum of three adsorption experiments were performed

on each substrate to account for variation in protein film thickness and an average measurement of Γ obtained. Verification of measurements by ellipsometry were previously determined by comparison of BSA adsorption on SiO_2 surfaces performed using a QCM technique [29].

2.5 Bacterial Attachment Assay

The attachment of *S. aureus* SH1000 [30] to sterile plain titanium (PT) coupons and TCFS coated superhydrophobic (SH) titanium coupons was performed using the method described previously [31, 32]. Where indicated, underwent protein adsorption with bovine fibrinogen (Fg) using the solution flow cell. Attachment assays were performed in 24 well plates in which coupons were immersed overnight in 3 ml of SH1000 cultures adjusted to $A_{600} = 0.2$ and subsequently incubated statically at 37°C for 1 h. The coupons were then removed from the plates and rinsed gently in $1 \times$ PBS to remove loosely adhered bacteria. To quantify the remaining attached bacteria, the coupons were placed in 1 ml sterile $1 \times$ PBS, vortexed for 5 min, sonicated gently for 2 min and then vortexed again for 2 min. The combination of vortexing and sonication was designed to detach bacterial cells from the surface of the coupon and to disrupt bacterial cell aggregates prior to serial dilution, plating onto brain heart infusion agar (Oxoid) and enumeration of colony forming units (CFUs). The number of CFUs in the inoculum was also determined and attachment retention was expressed as the percentage CFUs attached to the coupons relative to the number of bacteria in the inoculum. Each experiment was repeated three times and standard deviations are shown.

3 Results and Discussion

3.1 Plasma Polymerised Coatings

The siloxane and fluorosiloxane copolymer coatings were deposited onto silicon wafer substrates using an atmospheric pressure plasma jet system. To achieve surface coatings with different wetting properties the monomer chemistries, monomer flow rate, process gas and substrate to plasma source distance were systematically varied. The conditions established to achieve coatings with different wetting properties are given in Table 1. Both HMDSO and TCFS precursors were used to deposit hydrophobic and superhydrophobic coatings. Conditions applied to achieve superhydrophobic properties are marked with an asterisk in Table 1. The jet plasma was formed using a mixture of He/N_2 gas for hydrophobic and superhydrophobic coatings and He/O_2 for hydrophilic coatings. Superhydrophobic coatings were deposited at lower monomer flow rates,

Table 1 Deposition parameters used to form plasma polymer films with varying surface wetting properties

Monomer	Monomer flow rate ($\mu\text{l}/\text{min}$)	Process gas			Substrate to source distance (mm)
		He (l/min)	N ₂ (ml/min)	O ₂ (ml/min)	
TEOS	5	5	0	50	6
HMDSO	5	5	50	0	4
TCFS	5	5	50	0	4
HMDSO*	3	5	70	0	4
TCFS*	3	5	70	0	4

*Conditions used to achieve superhydrophobic wetting properties

which as previously reported has the effect of increasing surface roughness which results in the formation of a coating with a nano-textured morphology [33]. The deposition of hydrophilic coatings at higher monomer flow rates has been previously reported using this system [34]. In the current study, however, TEOS is deposited using lower monomer flow rates and each deposition pass is followed by a plasma treatment step (He/O₂) in the absence of any precursor monomer. This resulted in the formation of a superhydrophilic coating exhibiting complete surface wetting properties with no hydrophobic recovery observed over a 6 month period of sample storage under ambient room temperature conditions.

3.2 Surface Analysis

The water contact angle and surface energy measurements of the deposited coatings are shown in Fig. 1. TEOS coatings deposited from a He/O₂ plasma exhibit complete surface wetting with water contact angles of $<5^\circ$ and an average surface energy of 73 mJ m^{-2} . Water contact angle on uncoated silicon substrates had an average measurement of 24° with a calculated average surface energy of 65 mJ m^{-2} . Both HMDSO and TCFS coatings deposited at

$5 \mu\text{l min}^{-1}$ exhibited hydrophobic properties, with the fluorinated siloxane TCFS coating having a lower surface free energy. Both the HMDSO* and TCFS* coatings deposited using $3 \mu\text{l min}^{-1}$ exhibited water contact angles $>150^\circ$ and with respective surface energies of 1.2 and 0.8 mJ m^{-2} . Both of these coatings have the combination of nano textured surface morphology and hydrophobic chemistry necessary to achieve superhydrophobic performance [35] and exhibit surface energy values much lower than the other surface coatings.

The OWRK method used to analyse surface energy considers surface energy in terms of both polar and dispersive contributions. The polar component is assumed to be the sum of the polar, hydrogen, inductive and acid–base interactions and the dispersive component considers Van der Waals attractive interactions resulting from the interactions of instantaneous multipoles. These separate components of the surface energy measurements are shown in Fig. 2.

In Fig. 2 it can be seen that the relatively high polar and dispersive components in the hydrophilic region are contrasted by very low figures in the superhydrophobic region. In the intermediate hydrophobic region there is also a relatively low polar component but still quite a high

Fig. 1 Water contact angle and surface energy measurement on uncoated and plasma polymer coated silicon substrates. Values represent the average of five different measurements and standard deviations are indicated

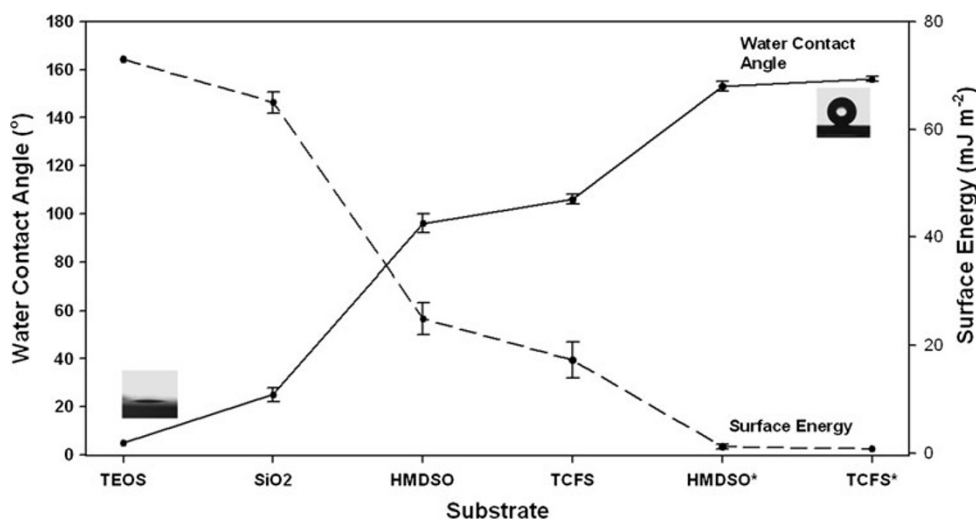
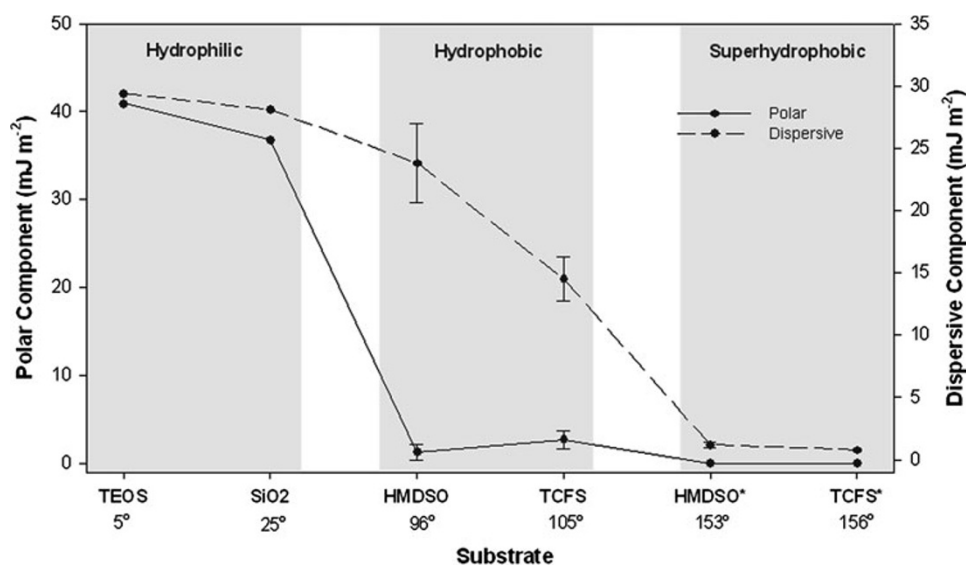


Fig. 2 Polar and dispersive contributions to surface free energy measurements on each test substrate. Polar components are assumed to be the sum of hydrogen, inductive and acid–base interactions and dispersive components the sum of Van der Waals interactive forces



dispersive contribution to surface free energy. In this region, the dispersive component is the larger contributing factor to surface energy. Despite similar polar interactions between the siloxane and fluorinated siloxane coating in the hydrophobic region, the dispersive component on the TCFS surface is substantially lower than on the siloxane HMDSO surface. A summary of the data obtained via contact angle measurement is given in Table 2.

Coatings thicknesses were measured to be between 100 and 285 nm, with superhydrophobic coatings exhibiting the greatest thickness. As expected, the uncoated silicon wafers were found to have a 2 nm native oxide layer thickness. The morphology and roughness of each of the surfaces was examined by optical profilometry. Thickness and roughness statistics are given in Table 3 and a comparison of hydrophobic and SH HMDSO and TCFS morphology is shown in Fig. 3. Both hydrophilic TEOS coatings and hydrophobic HMDSO coatings were shown to exhibit a very smooth surface morphology, with low R_a and R_q values. The similar R_a and R_q measurements are indicative of a homogenous surface morphology. Superhydrophobic HMDSO* coatings

Table 2 Water contact angle and surface energy of siloxane, fluorosiloxane and SiO₂ substrates used for protein adsorption studies

Coating	Water contact angle (°)	Surface energy (mJ m ⁻²)	Polar (mJ m ⁻²)	Dispersive (mJ m ⁻²)
TEOS	<5	71.3	40.9	29.4
SiO ₂	24	64.9	36.8	28.1
HMDSO	96	25.1	1.3	23.8
TCFS	106	17.2	2.7	14.5
HMDSO*	154	1.2	0.03	1.2
TCFS*	156	0.8	0.02	0.79

All values represent average measurements with a minimum of five measurements taken for each surface

Table 3 Average thickness and surface roughness of coatings

Coating	Thickness (nm)	Roughness (nm)	
		R_a	R_q
TEOS	125	5	6
SiO ₂	2	2	3
HMDSO	100	3	4
TCFS	145	34	44
HMDSO*	285	27	34
TCFS*	250	28	47

deposited at a flow rate of 3 $\mu\text{l min}^{-1}$ exhibited much higher roughness statistics. As outlined earlier, superhydrophobic coatings were deposited by reducing the precursor monomer flow rate into the plasma discharge and reducing the substrate to plasma source distance. This effectively increases the ratio of reactive plasma species to precursor monomer molecules and alters the gas flow dynamics by reducing the rate at which the process gas can exit the discharge tube. This leads to an increase in the number of fragmentation reactions occurring in the plasma discharge and results in a highly textured morphology as demonstrated in Fig. 3. The increase in surface roughness of siloxane films due to particulate formation in atmospheric plasma discharges has previously been observed [33, 36]. The line scan comparison in Fig. 4 shows surface feature height variation of <5 nm on the smooth HMDSO coating, while peak to trough height variation on the superhydrophobic coating shows differences between 10 and 100 nm on individual surface features.

TCFS coatings deposited at a flow rate of 5 $\mu\text{l min}^{-1}$ do not exhibit the same smooth morphology as HMDSO coatings deposited at the same flow rate. The TCFS surface exhibits an inhomogeneous surface roughness. This may be explained by the greater volatility (higher vapour pressure)

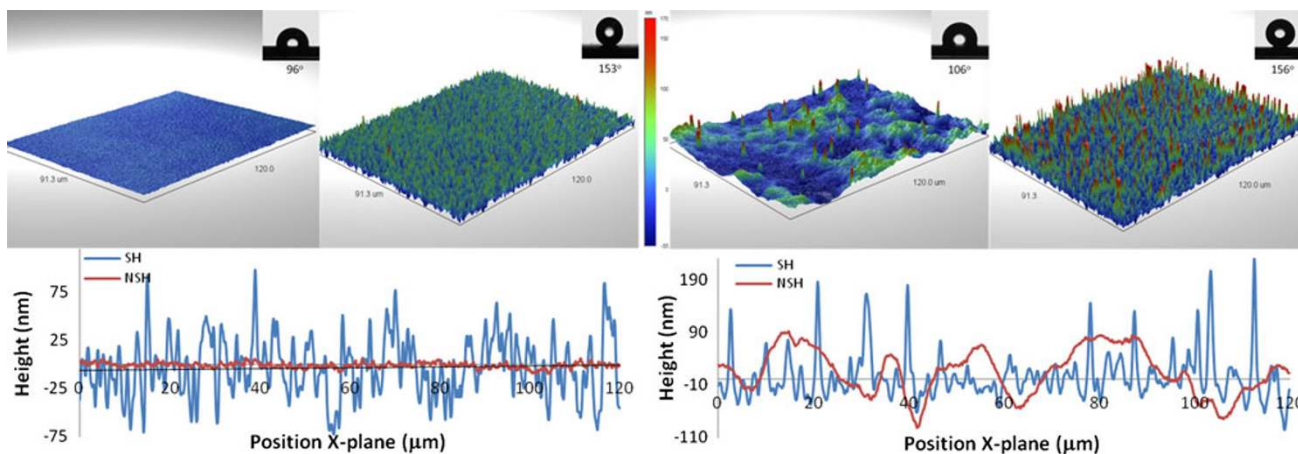
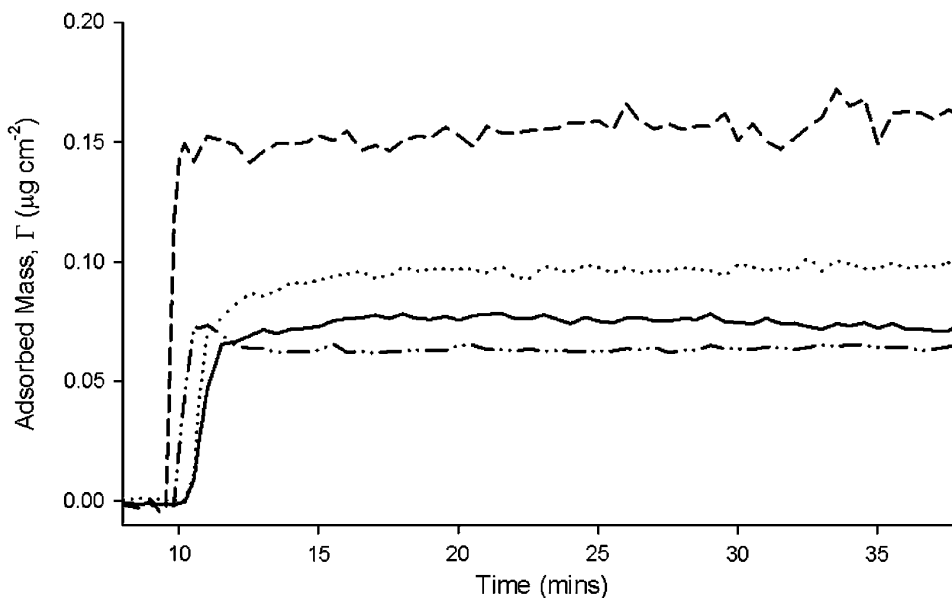


Fig. 3 Surface morphology and line scan of superhydrophobic (SH) and non-superhydrophobic (NSH) HMDSO coatings (*left*) and TCFS coatings (*right*)

Fig. 4 Adsorption profiles of BSA on TEOS (*solid line*), SiO₂ (*dotted line*), HMDSO (*dashed line*), and TCFS (*dashed dotted line*) surfaces



of the TCFS mixed monomer chemistry which also has a heavier molecular weight and greater chain length. These factors might more readily enable the formation and nucleation of larger particulates in the plasma discharge when compared to HMDSO. The superhydrophobic TCFS* coating deposited at a flow rate of 3 μl min⁻¹ also exhibits a greater variation in surface roughness than the superhydrophobic HMDSO* coatings. This coating exhibits protrusion features with peak to trough heights as high as 250 nm surrounded by smaller features with peak to trough heights of approximately 40 nm.

3.3 Coating Chemistry

To confirm retention of monomer chemistry in the plasma polymerised films, FTIR analysis on each of the coatings was performed. The infrared spectra of the coatings

deposited from the HMDSO precursor were dominated by a feature around 1,050 cm⁻¹ which can be attributed to the asymmetric Si–O–Si stretch [18]. In the case of the superhydrophobic coating, this peak was shifted to higher wavenumbers which may be a result of an increase in SiO_x stoichiometry. Peaks at 1,265, 1,350 and 2,965 cm⁻¹ were identified and assigned to Si–(CH)_x stretch and CH₃ asymmetric stretch, respectively. A broad peak between 3,200 and 3,550 cm⁻¹ was attributed to the SiOH functional group. The relative intensity of the CH₃ peak and SiOH band with respect to the Si–O–Si was reduced in the superhydrophobic coating. The infra-red spectra of the atmospheric plasma deposited coatings of TMCTS, PFOTES and combination TCFS were also determined. Coatings deposited from each of the monomers showed retention of all major spectral bands after plasma polymerisation. Spectral bands present in coatings deposited

from each of the monomers were identified in the copolymer spectrum also and were found to be in agreement with those reported previously concerning plasma polymerisation of both the TMCTS monomer [37] and the PFOTES monomers [38].

3.4 In Situ Ellipsometry Analysis of Protein Adsorption

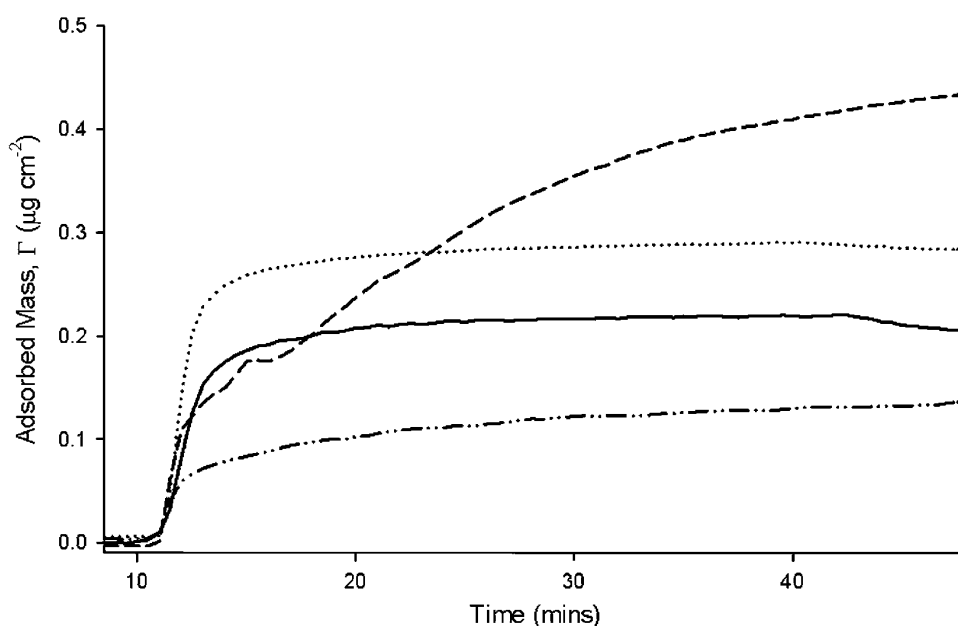
Protein adsorption on each of the surfaces was monitored by spectroscopic ellipsometry analysis. The measurements were carried out in situ using the liquid flow cell. The stability of the plasma deposited coatings was assessed by passing the PBS solution through the cell for 10 min prior to the introduction of the protein solution. After introduction of the protein solution there was an immediate shift from the baseline phase (Δ) signal which relates directly to a change in thickness at the substrate [39]. Spectroscopic data relating to both the change in Δ and change in Ψ were recorded. A Cauchy model was fit to these changes and a determination of the adsorbed protein film thickness (d_{el}) was made. The adsorbed amount of protein per unit area, or surface concentration, Γ was then calculated.

Typical adsorption profiles of BSA onto coated and uncoated wafer substrates are compared in Fig. 4. The adsorption of BSA is a relatively fast process, influenced by the surface binding affinity and diffusion rate of the protein through the solution. Immediately after introduction of the protein at 10 min, nearly full coverage on each of the surfaces is observed. A slow, further increase in adsorption is then observed to occur over a further 30 min period. The data shows an increase in Γ with increasing water contact angle, with respect to the TEOS, SiO₂ and

HMDSO substrates. The highest level of adsorption is seen to occur on the hydrophobic HMDSO surface where there is a large interfacial free energy between the substrate and water molecules, which protein molecules readily displace, reducing in the interfacial free energy. The adsorbed amount of $0.15 \mu\text{g cm}^{-2}$ is in agreement with results obtained by Lok et al. who measured the same surface saturation concentration for BSA on polymerised polydimethylsiloxane (PDMS) surfaces by total internal reflection fluorescence spectroscopy analysis [40]. Protein surface concentration on the TCFS surface, however, is lower than any of the other substrates despite its hydrophobic properties. As indicated by surface energy data, the dispersive component of surface energy is lower in the hydrophobic TCFS coating. This indicates that weak Van der Waals interactive forces may play a more significant role than polar interactions at the lower surface energy regimes. These short range forces also play an important role in stabilising protein molecules when they interact with other molecules or surfaces in the aqueous environment. The addition of fluorocarbon groups has the effect of reducing these interactions which may explain this reduction in protein binding on these hydrophobic surfaces.

Typical Fg adsorption plots are shown in Fig. 5. The average level of protein adsorption on each surface follows the same trend as BSA on each of the respective surfaces. After introduction of Fg the transition to saturation occurs over a period of 2–3 min on most of the surfaces. This longer initial adsorption rate when compared to BSA is a result of both a lower solution concentration and the larger molecular weight of the Fg molecule, which reduces diffusion rate of the protein through the solution. The adsorbed amount of Fg was found to be more than twice that of

Fig. 5 Adsorption profiles of Fg on TEOS (solid line), SiO₂ (dotted line), HMDSO (dashed line), and TCFS (dashed dotted line) surfaces



BSA on each of the respective surfaces investigated, indicative of its larger size and the greater flexibility inferred by its more elongated structure. The adsorbed amount was shown to increase with surface hydrophobicity with respect to TEOS, SiO₂ and HMDSO surfaces, while the fluorinated siloxane surface again exhibited the lowest adsorbed amount of about 1 μg cm⁻². The adsorbed Fg surface concentration of 0.28 μg cm⁻² on SiO₂ is consistent with data from Malmsted [14] who measured 0.29 μg cm⁻² and Yaseen [41] who measured a value of 0.3 μg cm⁻² on SiO₂ surfaces. The highest adsorbed amount of 0.46 μg cm⁻² on the hydrophobic HMDSO surface is in close agreement to results by Lok [40] who measured as adsorbed amount of 0.40 μg cm⁻² for Fg on PDMS siloxane surfaces. The slowest rate of Fg saturation is also observed on the hydrophobic HMDSO surface. Although there is a greater affinity for binding on the hydrophobic surface, this promotes the attachment of more Fg molecules, which may undergo surface reorientation after initial adsorption facilitating a slower surface saturation rate. The adsorption dynamics of Fg on HMDSO show a different profile shape to those observed on each of the other surfaces. The rate of saturation appears to slow until a time period of approximately 16 min, at which point the rate of saturation increases again. Fg is a larger more flexible protein than BSA, as such this change in adsorption dynamics may be indicative of a change in structure of the adsorbed layer. Multiple adsorption tests were carried out for each of the surfaces examined and the average protein surface concentration obtained. The average data can be seen in Fig. 6. The plot shows the general trend of increasing surface concentration with increasing contact angle, apart from on the TCFS surface which shows reduced adsorption with respect to both proteins investigated. Kumar et al. [42] also identified reduced protein

(albumin) adsorption on fluorocarbon surfaces, using a similar perfluorinated monomer to this study. While the current study considers the adsorption extent on a range of test surfaces, a study by Kiaei et al. which concerned the measurement of protein adsorption strength, identified stronger binding after SDS elution on fluorinated surfaces (tetrafluoroethylene) when compared to non fluorinated hydrophobic surfaces.

3.5 Analysis of Protein Adsorption and Bacterial Attachment on Superhydrophobic Surfaces

Figures 4 and 5 do not include adsorption dynamics on SH surfaces as it was not possible to fit an optical model to calculate a value for d_{ei} due to high variation in spectral data resulting from the textured nature of the SH surface morphology. A comparison, however, of the adsorption profiles on hydrophobic and superhydrophobic surfaces can be obtained by monitoring changes in phase signal (Δ) over time. The graphs shown in Fig. 8 compare changes in Δ at a fixed wavelength of 508 nm during adsorption experiments for BSA and Fg onto hydrophobic and superhydrophobic TCFS surfaces. The Δ change relates directly to a change in layer thickness and so can be used to give an indication of the amount of protein adsorbing to the substrate.

As shown in Fig. 7, there is a minor change in Δ on the SH surfaces indicating a low level of protein adsorption, which was also observed on the HMDSO* coatings. This resistance to protein adsorption is supported by results obtained by Koc et al. [43], who showed a reduction in protein binding on SH surfaces exposed to flow shear forces, while Khorasani et al. [44] also observed a reduction in serum protein adsorption and improved haemocompatibility on SH textured surfaces. Consistent with our data, Crick et al. [45] also observed a reduction in attachment of *S. aureus* and *Escherichia coli* on superhydrophobic coatings formed from silicone elastomers. The reduction in protein attachment to these surfaces would greatly alter the mechanism and sensitivity of cellular interactions with the coated surface when compared to a surface fully covered by a protein layer.

Protein adsorption experiments performed on SH surfaces using a QCM technique did not provide comparative data, as the structure and viscoelastic properties of the textured SH surface resulted in a decoupling of the coating from the driven sensor surface. Alternative confirmation of results obtained by ellipsometry which indicated minimal protein attachment to superhydrophobic surfaces was facilitated by bacterial attachment studies. Bacterial interactions with implanted biomaterials represent the first step in the development of biofilm-associated, device-related infections [46]. Surface hydrophobicity plays an important

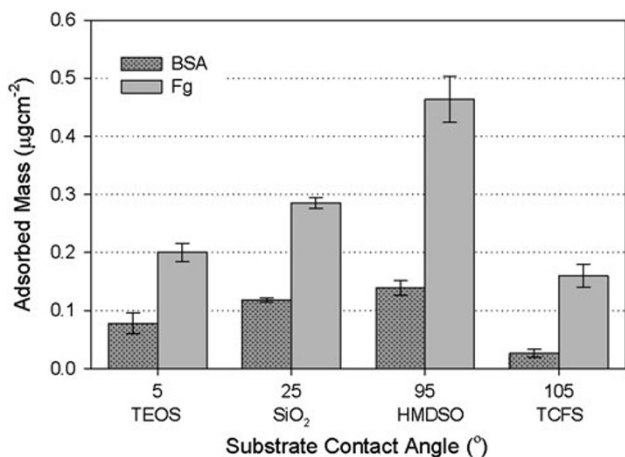


Fig. 6 Average adsorbed protein mass on each of the examined surfaces. Data represents a minimum of three tests for each surface examined and standard deviations are indicated

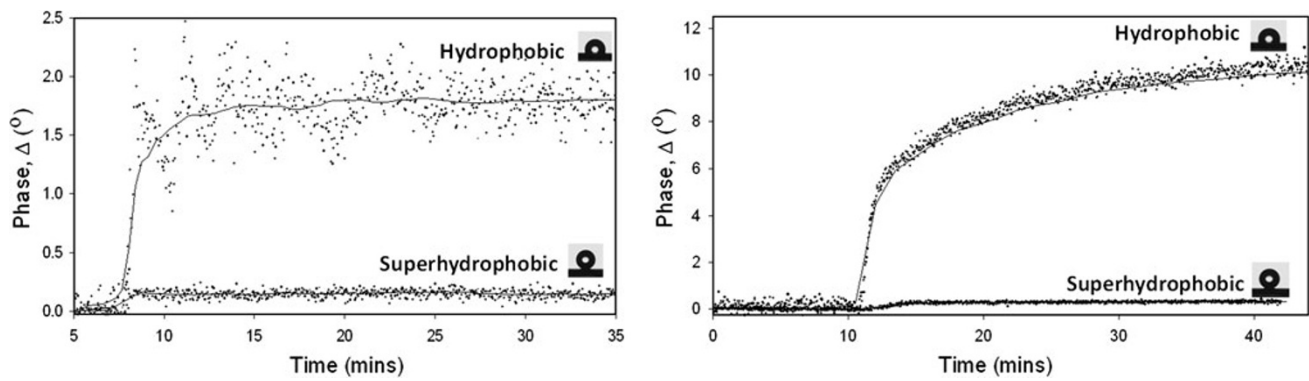
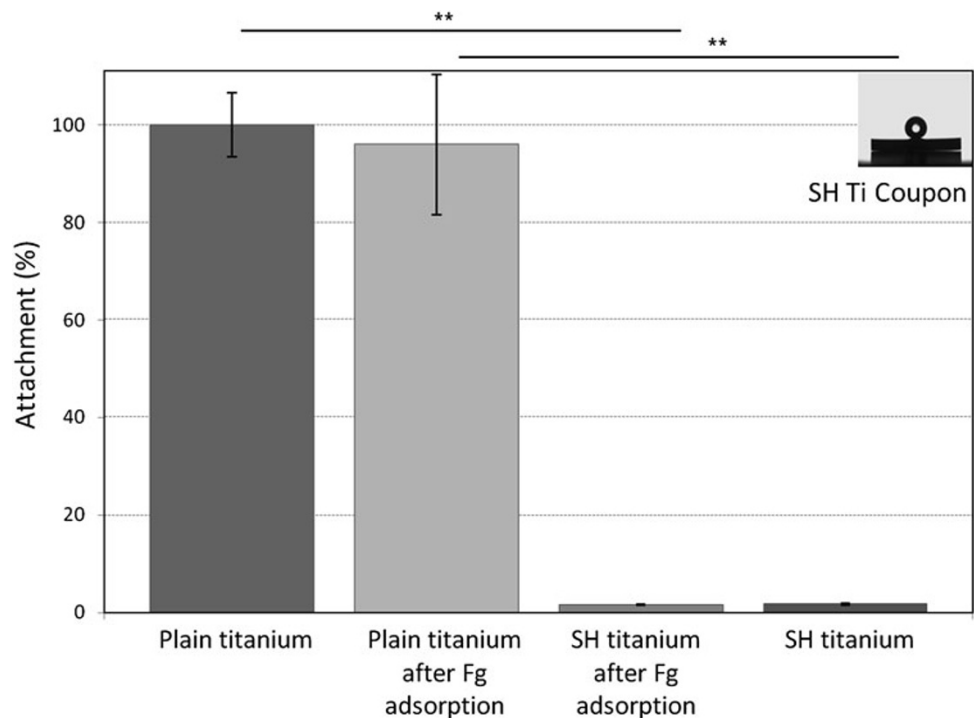


Fig. 7 Adsorption profiles of BSA (left) and Fg (right) on hydrophobic and superhydrophobic TCFS coatings

Fig. 8 Attachment of *S. aureus* SH1000 to Fg-coated and uncoated plain titanium and fluorosiloxane-coated superhydrophobic (SH) titanium. Attachment is expressed as the % cells attached. The attachment rates of SH1000 to uncoated plain titanium, Fg-coated SH titanium and uncoated SH titanium were compared to Fg-coated plain titanium, which this was assigned a value of 100 %. Experiments were repeated three times and standard deviations indicated. Asterisks denotes a significant difference ($P < 0.001$)



role in these interactions as does the conditioning film of serum and tissue proteins such as Fg and Fn, which is rapidly deposited on implanted biomaterials [46]. Bacterial pathogens express surface proteins that promote binding to Fg, Fn and a range of other serum and extracellular matrix proteins [46]. Thus, bacterial attachment experiments were carried out using an *S. aureus* (SH1000), which is known to bind specifically to Fg before and after protein adsorption experiments to identify any potential increase in bacterial attachment due to an adsorbed protein layer. It is hypothesised that SH coatings may both directly and indirectly (by limiting the deposition of serum and tissue proteins) reduce bacterial interactions with implanted materials.

To investigate this, the attachment of *S. aureus* onto plain titanium (PT) and TCFS* coated superhydrophobic (SH) titanium attachment studies were carried out both

before and after protein adsorption experiments. These results revealed that *S. aureus* cells attached at a significantly higher rate to PT than to SH titanium (Fig. 8). Furthermore the attachment of *S. aureus* to Fg 'treated' SH titanium was not significantly higher than the attachment to the uncoated SH titanium, indicating that there is little presence of an adsorbed protein layer. This is consistent with the ellipsometry data which indicated reduced Fg adsorption to the SH surface (Fig. 8). Considered together this data suggests that SH surfaces have the potential to limit bacterial interactions with implanted biomaterials and reduce protein adsorption.

This reduced protein and bacterial attachment may be attributed to the combined low surface energy chemistry and nano-textured morphology of the superhydrophobic coating. This chemistry and structure creates a barrier to

wetting by trapping pockets of air in the nano-scale morphology, which in effect presents a reduced surface area onto which protein molecules can diffuse from the flowing solution.

4 Conclusions

In situ adsorption of serum proteins has been investigated on plasma polymer surfaces deposited with wetting properties ranging from superhydrophilic to superhydrophobic. While reduced protein adsorption on superhydrophilic siloxane coatings was observed when compared to hydrophobic surfaces, much greater reductions were observed on superhydrophobic coatings. Hydrophobic siloxane coatings ($\theta = 95^\circ$) deposited from the HMDSO monomer showed the highest level of protein adsorption. Hydrophobic fluorinated copolymer siloxane coatings ($\theta = 105^\circ$), however, were shown to reduce the adsorption of both BSA and Fg. A comparison of surface energy data showed reduced dispersive interactions (Van der Waals forces) on the copolymer fluorinated siloxane coating. While the data confirms that protein adsorption tends to occur more favourably on hydrophobic surfaces than on hydrophilic surfaces, this result indicates that the specific surface chemistry also plays an important role in determining protein surface interaction as protein structural stability after adsorption is influenced by forces other than polar interactions. Analysis of protein adsorption on superhydrophobic surfaces indicated a significant reduction when compared to all other surfaces. A study of bacterial interactions on these coatings also showed a resistance to bacterial attachment. This study also confirmed resistance to protein adhesion on the superhydrophobic surface as indicated by minimal bacterial attachment both before and after protein adsorption trials.

Acknowledgments This work is supported by Science Foundation Ireland under Grant 08/SRC/I1411.

Open Access This article is distributed under the terms of the Creative Commons Attribution License which permits any use, distribution, and reproduction in any medium, provided the original author(s) and the source are credited.

References

- Ratner BD, Castner DG (1997) Surface modification of polymeric biomaterials. Springer, New York
- Katsikogianni M, Misirlis Y (2004) Eur Cell Mater 8:37–57
- Harold AS (2004) Biophys Chem 112(2–3):117–130
- McClellan SJ, Franses EI (2005) Colloids Surf A 260(1–3): 265–275
- Zhang F, Kang ET, Neoh KG, Wang P, Tan KL (2001) Biomaterials 22(12):1541–1548
- Chu PK, Chen J, Wang L, Huang N (2002) Mater Sci Eng R Rep 36(5–6):143–206
- Favia P, d'Agostino R (1998) Surf Coat Technol 98(1–3): 1102–1106
- Schmidt DR, Waldeck H, Kao WJ (2009) Biol Interact Mater Surf, 1–18
- Arima Y, Iwata H (2007) Biomaterials 28(20):3074–3082
- Xie H-G, Li X-X, Lv G-J, Xie W-Y, Zhu J, Luxbacher T et al (2010) J Biomed Mater Res Part A 92A(4):1357–1365
- Sigal GB, Mrksich M, Whitesides GM (1998) J Am Chem Soc 120(14):3464–3473
- Xu L-C, Siedlecki CA (2007) Biomaterials 28(22):3273–3283
- Lee JH, Lee HB (1993) J Biomater Sci Polym Edition 4(5): 467–481
- Malmsten M (1995) Colloids Surf B 3(5):297–308
- Nygren H, Alaeddin S, Lundström I, Magnusson K-E (1994) Biophys Chem 49(3):263–272
- Ishizaki T, Saito N, Takai O (2010) Langmuir 26(11):8147–8154
- Tamada Y, Ikada Y (1993) J Colloid Interface Sci 155(2):334–339
- Yasuda T, Ishizuka K, Ezoe M (2008) IEEEJ Trans Electr Electron Eng 3(3):290–296
- Huang S-L, Ou C-F, Lai J-Y (1999) J Membr Sci 161(1–2):21–29
- Roach P, Farrar D, Perry CC (2005) J Am Chem Soc 127(22): 8168–8173
- Goyal DK, Subramanian A (2010) Thin Solid Films 518(8): 2186–2193
- Berlind T, Tengvall P, Hultman L, Arwin H (2011) Acta Biomaterialia 7(3):1369–1378
- Boss J (2000) Biomaterials and bioengineering handbook. Marcel Dekker, Inc, New York, pp 1–94
- Slayter H (1983) Ann N Y Acad Sci 408(1):131–145
- Foster T, Höök M (2007) Infections associated with indwelling medical devices. ASM Press, Herndon, pp 27–39
- Albaugh J, O'Sullivan C, O'Neill L (2008) Surf Coat Technol 203(5–7):844–847
- Feijter JAD, Benjamins J, Veer FA (1978) Biopolymers 17(7):1759–1772
- Stenberg M, Nygren H (1983) Le Journal de Physique Colloques 44(C10):83–86
- Stallard C, McDonnell K, Donegan M, Dowling DP (2010) Evaluation of spectroscopic ellipsometry for the measurement of BSA protein adhesion on atmospheric plasma modified surfaces. ECNF conference March 22–25, Liege, Belgium
- Horsburgh MJ, Aish JL, White IJ, Shaw L, Lithgow JK, Foster SJ (2002) J Bacteriol 184(19):5457
- O'Neill E, Pozzi C, Houston P, Humphreys H, Robinson DA, Loughman A et al (2008) J Bacteriol 190(11):3835
- Houston P, Rowe SE, Pozzi C, Waters EM, O'Gara JP (2011) Infect Immun 79(3):1153
- O'Neill L, Herbert PAF, Stallard C, Dowling DP (2010) Plasma Process Polym 7(1):43–50
- Ramamoorthy A, Rahman M, Mooney DA, Don MacElroy JM, Dowling DP (2009) Plasma Process Polym 6(S1):S530–S536
- Onda T, Shibuichi S, Satoh N, Tsujii K (1996) Langmuir 12(9):2125–2127
- Schmidt-Szalowski K (2000) Plasmas Polym 5(3):173–190
- Yang S-H, Liu C-H, Su C-H, Chen H (2009) Thin Solid Films 517(17):5284–5287
- Seitz R, Brings R, Geiger R (2005) Appl Surf Sci 252(1):154–157
- Tompkins HG, McGahan WA (1999) Spectroscopic ellipsometry and reflectometry. Wiley, New York
- Lok BK, Cheng Y-L, Robertson CR (1983) J Colloid Interface Sci 91(1):104–116

41. Yaseen M, Salacinski H, Seifalian A, Lu J (2008) *Biomed Mater* 3:034123
42. Kumar V, Pulpytel J, Rauscher H, Mannelli I, Rossi F, Arefi-Khonsari F (2010) Fluorocarbon coatings via plasma enhanced chemical vapor deposition of 1H,1H,2H,2H-perfluorodecyl Acrylate-2, morphology, wettability and antifouling characterization. WILEY-VCH Verlag, pp 926–938
43. Koc Y, de Mello AJ, McHale G, Newton MI, Roach P, Shirtcliffe NJ (2008) *Lab Chip* 8(4):582–586
44. Khorasani MT, Mirzadeh H (2004) In vitro blood compatibility of modified PDMS surfaces as superhydrophobic and superhydrophilic materials. Wiley Subscription Services, Inc., A Wiley Company, New York, pp 2042–2047
45. Crick CR, Ismail S, Pratten J, Parkin IP (2011) *Thin Solid Films* 519(11):3722–3727
46. O’Gara JP (2007) *FEMS Microbiol Lett* 270(2):179–188